Supercapacitor Electrodes from Tubes-in-Tube Carbon Nanostructures

Hui Pan,*,† Chee Kok Poh,‡ Yuan Ping Feng,† and Jianyi Lin*,†,‡

Department of Physics, National University of Singapore, 2 Science Drive 3, Singapore 117542, Singapore, and Institute of Chemical and Engineering Sciences, 1 Pesek Road, Jurong Island, Singapore 627833, Singapore

Received June 7, 2007. Revised Manuscript Received October 1, 2007

Supercapacitors occupying a region between batteries and dielectric capacitors have been touted as a solution to the mismatch between the fast growth in power required by devices and the inability of batteries to efficiently discharge at high rates. Here, we report the electrochemical characterization of tubes-in-tube carbon nanostructures to investigate their application to supercapacitors. The average specific capacitance has been calculated for the cyclic voltammetric plots at 50 mV/s. The tubes-in-tube multiwalled carbon nanotubes consisting of outer nanotubes with an average outer diameter of 50 nm and inner nanotubes with diameters in the range of 3–10 nm exhibit an average capacitance of 203 F/g and a specific capacitance of 315 F/g at 0.35 V in 0.5 mol/L H_2SO_4. Pure electrostatic attraction in the double layer and faradic reaction in the pseudocapacitor are responsible for the supercapacitance. The specific surface area of the samples characterized by a nitrogen isotherm at 77 K reveals that the higher supercapacitance can be realized by modifying the pore size, pore-size distribution, and conductivity of the carbon nanomaterials.

The power requirements for a number of portable electronic devices have exceeded the capability of conventional batteries to such an extent that great attention is being focused on supercapacitors with higher power density and less reduction in energy density. Supercapacitors are electrochemical capacitors (ECs) formed by two polarizable electrodes, a separator and an electrolyte. The capacitance of a supercapacitor is the sum of double-layer capacitance and pseudocapacitance. Double-layer capacitance arises when a charge accumulation is achieved electrostatically on either side of the electrode and electrolyte interface, while pseudocapacitance is brought about by surface redox reaction. Electrode materials for ECs have been extensively studied because of the increasing demand for a new kind of energy storage device with high specific power and long durability.[1] This storage device can be used in digital telecommunication systems, uninterruptible power supplies for computers, pulse laser techniques, etc. These electrode materials include active carbons,[2–4] conducting polymers (such as polyacetylene, polypyrrole, and polyaniline),[5,6] oxides (such as RuO_2 and Co_3O_4),[7–9] and their composites. Recently, carbon nanotubes (CNTs) have been studied for electrochemical supercapacitor electrodes because of their unique properties, such as large surface area, superb chemical stability, flexibility, and high conductivity.[10–12] The capacitance values of CNTs strongly depend on the CNT purity and electrolyte,[13–15] as well as the functionalization of CNTs.[10,12,16,17] Another way to increase the capacitance of a CNT supercapacitor is to modify the CNTs with conducting polymers or oxides because conducting polymers and oxides are known to create pseudocapacitance through a faradic process.[18–21]

* Corresponding author. E-mail: phyph@nus.edu.sg; lin_jianyi@ices.a-star.edu.sg.
† National University of Singapore.
‡ Institute of Chemical and Engineering Sciences.

(1) Conway, B. E. *Electrochemical supercapacitors: scientific fundamentals and technological applications*; Kluwer Academic/Plenum: New York, 1999.
(2) Raymundo-Pinero, E.; Leroux, F.; Beguin, F. *Adv. Mater.* **2006**, *18*, 1877.
(3) Gamby, J.; Taberna, P. L.; Simon, P.; Fauvarque, J. F.; Chesneau, M. *J. Power Sources* **2001**, *104*, 109.
(4) Celzard, A.; Collas, F.; Mareche, J. F.; Furdin, G.; Rey, I. *J. Power Sources* **2002**, *108*, 153.
(5) Lota, K.; Khomenko, V.; Frackowiak, E. J. *J. Phys. Chem. Solids* **2004**, *65*, 295–301.
(6) Ryu, S. K.; Wu, X.; Lee, Y. G.; Chang, S. H. *J. Appl. Polym. Sci.* **2003**, *89*, 1300–1304.
(7) Chang, K. H.; Hu, C. C. *Electrochem. Solid State Lett.* **2004**, *7*, A466–A469.
(8) Rochefort, D.; Guay, D. J. *Alloys Compds.* **2005**, *400*, 257–264.
(9) Broughton, J. N.; Brett, M. J. *Electrochim. Acta* **2005**, *49*, 4439–4446.
(10) Niu, C.; Sichel, E. K.; Hoch, R.; Moy, D.; Tennent, H. *Appl. Phys. Lett.* **1997**, *70*, 1480–1482.
(11) Du, C.; Pan, N. *Nanotechnology* **2006**, *17*, 5314.
(12) Lee, J. Y.; An, K. H.; Heo, J. K.; Lee, Y. H. *J. Phys. Chem. B* **2003**, *107*, 8812–8815.
(13) Frackowiak, E.; Jurewicz, K.; Delpeux, S.; Beguin, F. *J. Power Sources* **2001**, *97*, 822–8252.
(14) Barisci, J. N.; Wallace, G. G.; Chattopadhyay, D.; Papadimitrakopoulos, F.; Baughman, R. H. *J. Electrochem. Soc.* **2003**, *150*, E409–E415.
(15) Barisci, J. N.; Wallace, G. G.; MacFarlane, D. R.; Baughman, R. H. *Electrochem. Commun.* **2004**, *6*, 22–27.
(16) Frackowiak, E.; Metenier, K.; Bertagna, V.; Beguin, F. *Appl. Phys. Lett.* **2000**, *77*, 2421–2423.
(17) Yoon, B. J.; Jeong, S. H.; Lee, K. H.; Kim, H. S.; Park, C. G.; Han, J. H. *Chem. Phys. Lett.* **2004**, *388*, 170–174.
(18) Zhou, C.; Kumar, S.; Doyle, C. D.; Tour, J. M. *Chem. Mater.* **2005**, *17*, 1997–2002.
(19) Hughes, M.; Chen, G. Z.; Shaffer, M. S. P.; Fray, D. J.; Windle, A. H. *Chem. Mater.* **2002**, *14*, 1610–1613.
(20) Downs, C.; Nugent, J.; Ajayan, P. M.; Duquette, D. J.; Santhanam, S. V. *Adv. Mater.* **1999**, *11*, 1028–1031.

10.1021/cm071527e CCC: $37.00
Published on Web 11/08/2007

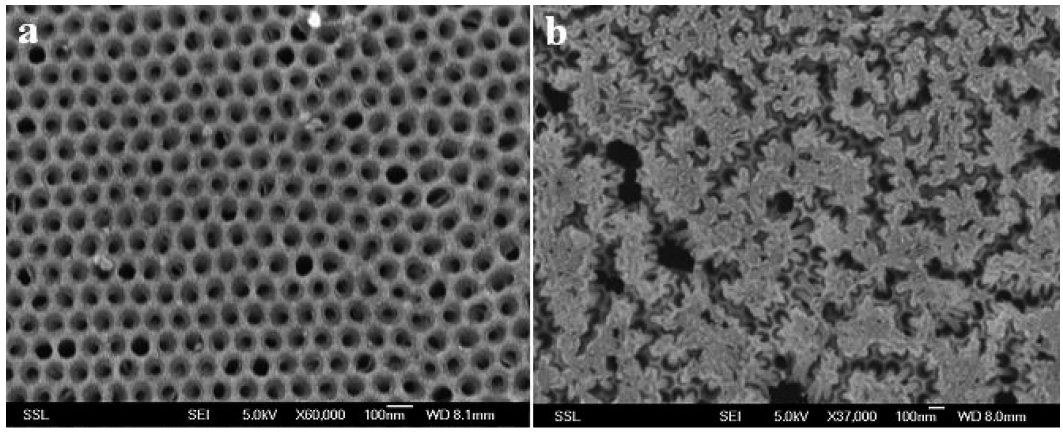

Figure 1. SEM images of AAO-based 50 nm MWCNTs after the first-step pyrolysis of C_2H_4: (a) before removal of the AAO template; (b) partial removal of the surface of the AAO template.

Here, we report that a high capacitance value of the supercapacitor based on tubes-in-tube CNTs can be realized. The CNTs with uniform diameters in this study were first produced by the template method, where anodic aluminum oxide (AAO) was used as the template because it can be easily produced by two-step anodization with uniform diameters of nanopores in the template. The tubes-in-tube CNTs were fabricated by the second pyrolysis of ethylene (C_2H_4) inside the CNTs with the template using a catalyst. It was noticed that the capacitance of the supercapacitor based on CNTs was strongly related to the CNTs' diameters and structures.

The tubes-in-tube multiwalled CNTs (TiT-MWCNTs) were fabricated by a two-step pyrolysis of C_2H_4 at higher temperature based on the AAO template. A modified two-step anodization was utilized to prepare the ordered AAO template.[22] The remaining Al was removed in a $CuCl_2$ solution. MWCNTs were produced by a first-step pyrolysis of C_2H_4. Generally, the growth of MWCNTs was carried out in a quartz reactor at 900 °C under a flow of Ar (95%) and a H_2 (5%) gas mixture at 100 sccm and by a one-step pyrolysis of C_2H_4 at 16 sccm without catalysts. The TiT-MWCNTs were produced by a second-step pyrolysis of C_2H_4. After the first-step pyrolysis of C_2H_4, the MWCNTs were produced within the nanopores of the AAO template. Then, they were immersed in a Ni_2SO_4 solution for 2 h to deposit the catalyst to the inner walls of the MWCNTs. Second-step pyrolysis was performed at the same conditions except the temperature was reduced to 700 °C to grow the TiT-MWCNTs using the AAO-based MWCNTs with a Ni catalyst within the MWCNTs. The MWCNTs and TiT-MWCNTs were released from the template using hydrofluoric and hydrochloric acids, cleaned to pH = 7 in distilled water, and vacuum-dried at 120 °C. The morphology of the CNTs was observed by scanning electron microscopy (SEM; JEOL JSM-6700F) and transmission electron microscopy (TEM; JEOL 2010F). The CNTs were characterized by Raman scattering (Renishaw 2000 system with 1 cm^{-1} resolution and 0.4 cm^{-1} reproducibility, at an excitation source of 514.5 nm). The specific surface area of the samples was characterized by a nitrogen isotherm at 77 K (NOVA 3200, Quantachrome Corp.) based on the Brunauer–Emmett–Teller (BET) method. The pore-size distribution was calculated using the Barrett–Joyner–Halenda (BJH) method.

Cyclic voltammetry (CV) measurements were performed in an electrochemical measurement unit (Solartron SI1280B), a combined electrochemical interface and frequency response analyzer, at room temperature with a scan rate of 50 mV/s. The working electrode was fabricated by casting a Nafion-impregnated sample onto a glassy carbon electrode. Typically, 4 mg of the sample dispersed in 0.5 mL of an aqueous ethanol solution (1:1, v/v) was sonicated for 15 min.[23] This sample was dropped onto the carbon electrode, which was then placed in a vacuum oven until the sample was totally dry for the CV measurement. The cast working electrode was then immersed in 0.5 mol/L H_2SO_4, which was deaerated with a high-purity nitrogen gas for electrochemical measurement. A Pt foil and a saturated calomel electrode were used as counter and reference electrodes, respectively. Five samples were used in our experiments for comparison. They included AAO MWCNTs (50 nm in diameter), AAO MWCNTs (300 nm), AAO TiT-MWCNTs (50 nm), AAO TiT-MWCNTs (300 nm), and commercial MWCNTs (20–40 nm), which were labeled as AM50, AM300, ATM50, ATM300, and CM20, respectively.

MWCNTs were normally confined within the pore channels because the alumina channel inner wall decomposes the hydrocarbon. Figure 1 is the SEM image of MWCNTs produced on the AAO template (50 nm) after the first-step pyrolysis of C_2H_4. Figure 1a clearly indicates that MWCNTs were within the nanopores in the template. The nanopores were widened, and the MWCNTs were exposed after the AAO template was partially etched, as indicated in Figure 1b. The exposed tips of the MWCNTs have equal length and are tangled together. The MWCNTs have a uniform diameter of about 50 nm. Figure 2 shows the SEM images of TiT-MWCNTs after total removal of the AAO template. The surface of the TiT-MWCNTs is

(21) Fang, W. C.; Chyan, O.; Sun, C. L.; Wu, C. T.; Chen, C. P.; Chen, K. H.; Chen, L. C.; Huang, J. H. *Electrochem. Commun.* **2007**, *9*, 239.

(22) Pan, H.; Lin, J.; Feng, Y.; Gao, H. *IEEE Trans. Nanotechnol.* **2004**, *3*, 462–467.

(23) Li, G.; Pickup, P. G. *J. Electrochem. Soc.* **2003**, *11*, C745–C752.

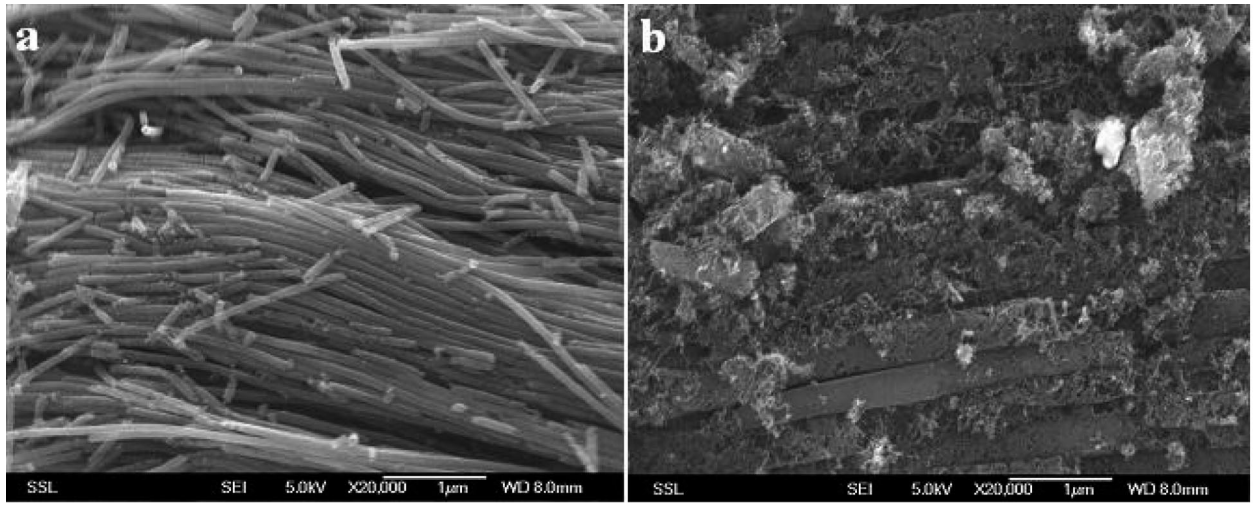

Figure 2. SEM images of AAO-based MWCNTs after the second-step pyrolysis of C_2H_4 with the AAO templates removed: (a) ATM50; (b) ATM300.

rough, with a lot of small pores. For 300 nm TiT-MWCNTs, it is clear that the MWCNTs (300 nm) confine a lot of smaller carbon CNTs. Some TiT-MWCNTs (300 nm) were broken and smaller CNTs were released from inside during the procedure to remove the AAO template in acid because of their poor graphitization (Figure 2b). The diameter of the smaller CNTs within the MWCNTs (300 nm) is about 30 nm. For 50 nm TiT-MWCNTs, the smaller CNTs within the MWCNTs (50 nm) are less than 10 nm in diameter, which was difficult to observe by SEM, as shown in Figure 2a, but was confirmed by TEM as discussed below.

Figure 3 shows the TEM images of AM50 and ATM50. For MWCNT produced by the first-step pyrolysis of C_2H_4, the channel is empty (Figure 3a) and the tube's wall is thinner. After the second-step pyrolysis of C_2H_4, the channel was filled with smaller CNTs (Figure 3b). Figure 3c shows that the diameter of inside CNTs is around 10 nm. Much smaller CNTs with diameters of less than 3 nm can be observed within the bigger MWCNTs, as indicated in Figure 3d. The difference in the diameters of inside CNTs was contributed to the different sizes of the Ni catalyst within the AAO-based MWCNTs. The existence of the inside tubes was confirmed by Raman scattering, as discussed in the following.

Raman spectra in Figure 4 show two characteristic peaks of MWCNTs, i.e., the G band around 1580 cm^{-1} and the D band at 1340 cm^{-1}, for all of the samples. The G band is related to the hybridization of sp^3 and the D band to that of sp^2. The graphitization of CNTs can be estimated by the intensity ratio of the D vs G band (I_D/I_G). The smaller the I_D/I_G ratio is, the higher the graphitization of CNTs. Obviously, the graphitization of all of the samples is low. Nevertheless, in Table 1, AM50 and ATM50 are generally better in graphitization than AM300, ATM300, and CM20. Also, the graphitization of the TiT-MWCNTs is better than that of the corresponding AAO-based CNTs because the catalyst-assisted inside CNTs produced in the second-step pyrolysis of C_2H_4 show better graphitization than the AAO-based CNTs (Table 1). The Raman scattering further indicated the formation of CNTs within the AAO-based MWCNTs. The graphitization level of CNTs is also related to the specific surface area and the average pore size of the carbon nanostructure as measured by BET.

The CV measurement is helpful in understanding the electrochemical performance on the electrode of the supercapacitor during charging and discharging processes. Figure 5a shows the CV plots of the samples in the aqueous solution of 0.5 mol/L H_2SO_4 at a scan rate of 50 mV/s. The CV plot of the background is almost a straight line at the middle of the figure, which indicates that the contribution of the background to our results is negligible. Two peaks on every CV plot for the five samples indicate the existence of the faradic processes. The charge storage in the faradic process is achieved by an electron transfer that produces chemical or oxidation state changes in the electroactive materials according to Faraday's law related to the potential.[1] The well-remarkable region with reversible faradic reactions is observed within the range of 0.2−0.4 V (Figure 5a). The redox peaks on the CV plots can be ascribed to oxygenated groups attached to the surface of the carbon nanostructures, such as OH^-.[24,25]

The voltammetric charge (q) integrated from a positive or negative sweep of CV plots can be used as an effective signal in determining the pseudocapacitance in redox transitions.[1] Accordingly, the average specific capacitance of the above-mentioned samples was estimated from the CV plots in Figure 5a by integrating the area under the current (per gram of the sample)−potential curve and then dividing by the sweep rate and the potential window according to the following equation:

$$C_{ave} = q/(\Delta V m) = \frac{1}{1.2mv}\int_{-0.2}^{1.0} i(V)\,dV \qquad (1)$$

where v is a constant of the sweep rate applied for the CV measurements, i.e., dV/dt, $i(V)$ is a current response depending on the sweep voltage, and the voltammetric charge is thus estimated as $q = \int_{-0.2}^{1.0}[i(V)/v]\,dV$. The sweep potential ($\Delta V$) is from −0.2 to 1.0 V. The average

(24) Ye, J. S.; Liu, X.; Cui, H. F.; Zhang, W. D.; Sheu, F. S.; Lim, T. M. *Electrochem. Commun.* **2005**, *7*, 249.
(25) Kim, Y. T.; Ito, Y.; Tadai, K.; Mitani, T.; Kim, U.-S.; Kim, H. S.; Cho, B. W. *Appl. Phys. Lett.* **2005**, *87*, 234106.

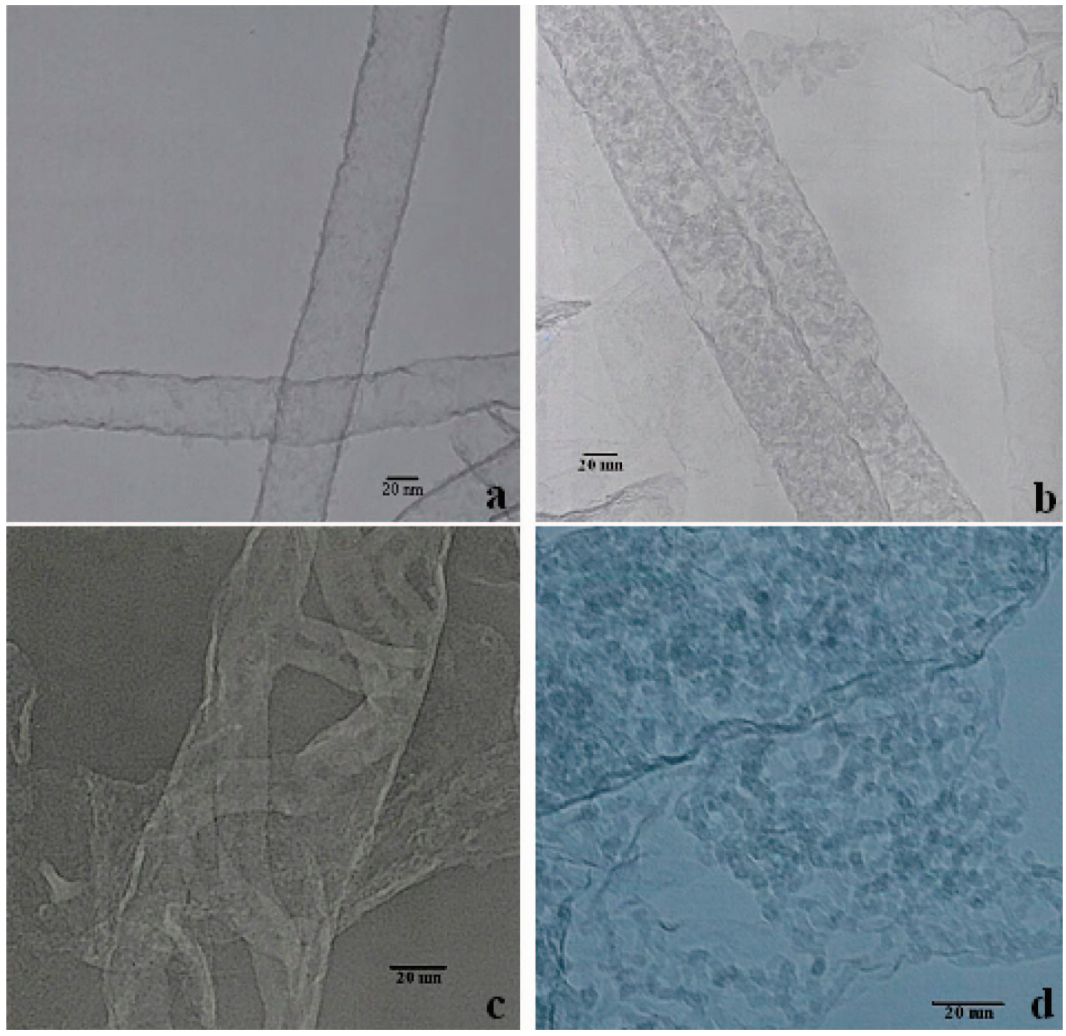

Figure 3. TEM images of AAO-based 50 nm MWCNTs after the first- and second-step pyrolyses of C_2H_4: (a) AM50; (b) ATM50; (c and d) fine view of ATM50.

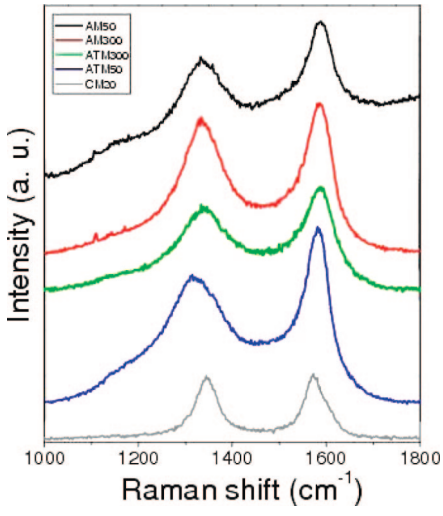

Figure 4. Raman spectra of the five samples.

specific capacitance of commercial CNTs (20–40 nm in diameter) is about 23 F/g, which was comparable to the value reported in the literature.[26] The average specific capacitances are 92, 29, 203, and 59 F/g for AM50, AM300, ATM50, and ATM300, respectively (Table 1). The average specific capacitance of ATM50 is about 8 times that for the commercial CNTs. The capacitances of AM50, AM300, and ATM300 are comparable to those of the MWCNTs, as reported in the literature[10,16,25] but are less than the maximum specific capacitance of the high-temperature-treated single-walled CNTs (SWCNTs, 180 F/g).[27] The capacitance of ATM50 is better than those of other samples and SWCNTs. The existence of the redox peaks on the CV plot of ATM50 indicated that the CV shape is not indicative of an ideal double-layer capacitor. The electrode of ATM50 was tested by the CV measurement for 5000 cycles. We did not observe a decrease of the specific capacitance, which indicated the cycling stability of ATM50 (Figure 5b). The larger slopes ($\Delta I/\Delta V$) demonstrated by the boxes in Figure 5b indicate that ATM50 has faster charging and discharging responses to the applied potential. The specific capacitance (C_s) and charge (q) are potential-dependent (see the Supporting Information). For the sample ATM50, C_s is in the range of 170−315 F/g.

(26) Liu, T.; Sreekumar, T. V.; Kumar, S.; Hauge, R. H.; Smalley, R. E. *Carbon* **2003**, *41*, 2440–2442.

(27) An, K. H.; Kim, W. S.; Park, Y. S.; Choi, Y. C.; Lee, S. M.; Chung, D. C.; Bae, D. J.; Lim, S. C. *Adv. Mater.* **2001**, *13*, 497.

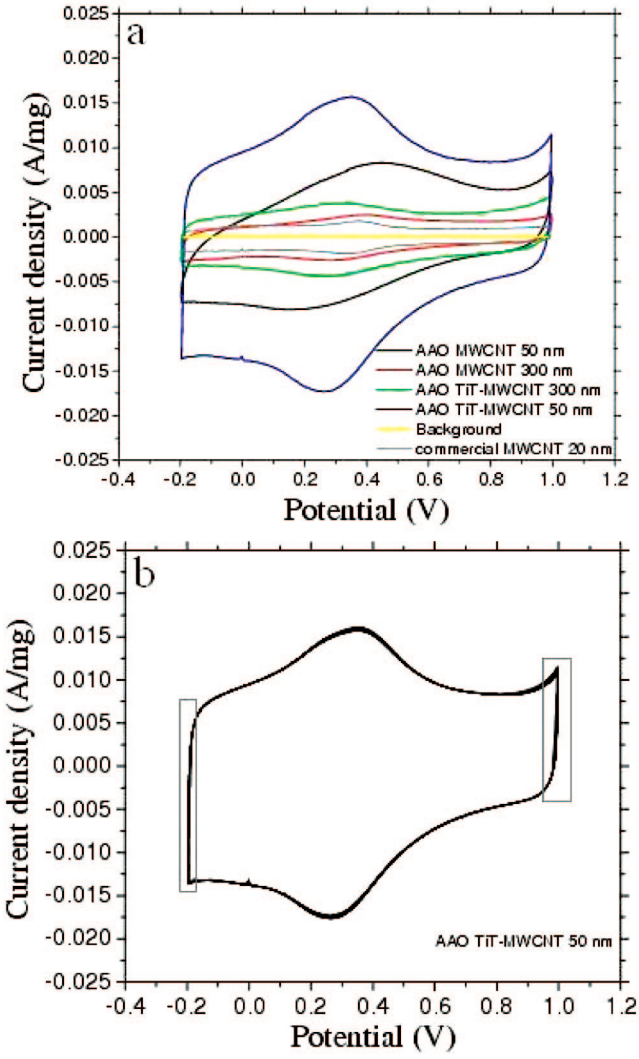

Figure 5. CV plots in 0.5 M H_2SO_4 at a scan rate of 50 mV/s for (a) the five samples with one cycle and (b) ATM50 for 5000 cycles.

Table 1. Specific Surface Area, Average Pore Size, and Capacitance of the Carbon Nanomaterials

	CM20	AM50	AM300	ATM50	ATM300
I_D/I_G	1.03	0.86	0.92	0.74	0.84
specific area (m^2/g)	136	649	264	500	390
average pore diameter (nm)	8.8	3.9	7.4	5.2	9.1
capacitance (F/g)	17	91	23	203	53

The capacitance of carbon-based electrochemical supercapacitors depends on two kinds of accumulated energy:[1] the electrostatic attraction in electrical double-layer capacitors (EDLCs) and faradic reactions induced pseudocapacitance. The amount of electrical charge accumulated due to electrostatic attraction in EDLC depends on the area of the electrode/electrolyte interface that can be accessed by the charge carriers. Therefore, the higher surface area of the electrode material could lead to higher capacitance if the area can be fully accessed by the charge carriers. However, the surface area is hardly accessible if it consists of micropores (<2 nm).[28] However, a higher surface area does not always result in higher capacitance because the capacitance depends on the pore size and pore-size distribution. The average pore diameters of all samples are larger than 2 nm (Table 1). Also, the smaller specific area leads to a larger average pore diameter with the exception of ATM300 (Table 1). The pore-size distributions for AM50 and ATM50 are narrow and show that the dominant pore diameter is about 3.9 nm. However, the pore-size distributions for other samples are broad and extend to larger size, although the dominant pore diameter is about 2 nm for other samples (Figure 6). The smaller average pore sizes in AM50 and ATM50 measured by BET are consistent with the Raman scattering measurement because they have better graphitization than other samples (Figure 4). It is noticed that the average specific capacitance for AM50 and ATM50 is larger than those of other samples. Also, it was found that the average specific capacitance increases with an increase of the specific surface area with the exception of ATM50. The electrical conductivity is one of the factors that affects the capacitance. It should be mentioned that the higher the surface area, the poorer the conductivity should be. This should be one of the reasons for the capacitance of ATM50 being larger than that of AM50.

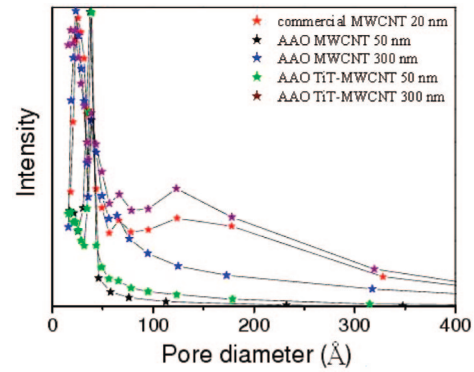

Figure 6. Pore-size distribution calculated using the BJH method.

Pseudocapacitance induced by faradic reactions also contributes to the capacitance, which depends on the surface functionalization of the carbon nanostructures. The redox peaks in the CV plots indicate the existence of oxygenated groups (OH^-) on the surface of the carbon nanostructures, which leads to the remarkable pseudocapacitance. The redox reaction (faradic process) can be considered as follows:[16,25]

$$>C-OH \leftrightarrow C=O + H^+ + e^- \quad (2)$$

$$>C=O + e^- \leftrightarrow >C-O^- \quad (3)$$

The pseudocapacitance arises from the quick faradic charge-transfer reactions. Obviously, the pseudocapacitance is strongly related to the pore size, pore-size distribution, and conductivity of the carbon materials. It can be noticed that ATM50 shows the highest average specific capacitance because of its higher surface area, better pore-size distribution, and conductivity as analyzed in the EDLC.

In summary, we synthesized the tubes-in-tube carbon nanostructures by a simple two-step pyrolysis of C_2H_4 based on the AAO template. The tubes-in-tube carbon

(28) Frackowiak, E.; Beguin, F. *Carbon* **2001**, *39*, 937–950.

nanostructures exhibit higher supercapacitance and faster charging and discharging responses to the applied potential compared with commercial CNTs and AAO-based MWCNTs produced by one-step pyrolysis of C_2H_4. The smaller diameter TiT-MWCNTs show higher supercapacitance than the larger diameter TiT-MWCNTs. The higher supercapacitance of ATM50 is contributed to its larger surface area, better pore-size distribution, and high conductivity. These tubes-in-tube carbon nanostructures should be promising candidates for the power requirements of high-power devices.

Supporting Information Available: Figure of the intermediate results on the capacitance and charge calculated using $dq = i\,dt/m = i\,dV/mv$ and $C_s = dq/dV$. This material is available free of charge via the Internet at http://pubs.acs.org.

CM071527E